Experimental and Theoretical Investigation of Thiazolyl Blue as a Corrosion Inhibitor for Copper in Neutral Sodium Chloride Solution

Li Feng [1], Shengtao Zhang [1,2,*], Yujie Qiang [1], Yue Xu [1], Lei Guo [3,*] , Loutfy H. Madkour [4] and Shijin Chen [5]

[1] School of Chemistry and Chemical Engineering, Chongqing University, Chongqing 400044, China; fengli_cqu@163.com (L.F.); yqiang_cqu@163.com (Y.Q.); cqtanjc@163.com (Y.X.)
[2] Material Corrosion and Protection Key Laboratory of Sichuan province, Zigong 643000, China
[3] School of Material and Chemical Engineering, Tongren University, Tongren 554300, China
[4] Chemistry Department, Faculty of Science and Arts, Al Baha University, Baljarashi 65635, Saudi Arabia; loutfy_madkour@yahoo.com
[5] Bomin Electronics Ltd., Meizhou 514021, China; fwjshen@163.com
*   Correspondence: stzhang@cqu.edu.cn (S.Z.); cqglei@163.com (L.G.)

Abstract: The anticorrosion effect of thiazolyl blue (MTT) for copper in 3% NaCl at 298 K was researched by electrochemical methods, scanning electron-microscopy (SEM), and atomic force microscopy (AFM). The results reveal that MTT can protect copper efficiently, with a maximum efficiency of 95.7%. The corrosion inhibition mechanism was investigated by X-ray photoelectron spectroscopy (XPS), Fourier transform infrared spectral (FT-IR), and theoretical calculation. The results suggest that the MTT molecules are adsorbed on metal surface forming a hydrophobic protective film to prevent copper corrosion. It also indicates that the MTT and copper form covalent bonds. The molecular dynamic simulation further gives the evidence for adsorption. The adsorption isotherm studies demonstrate that a spontaneous, mixed physical and chemical adsorption occurs, which obeys Langmuir adsorption isotherm. The present research can help us better understand the corrosion inhibition process and improve it.

1. Introduction

Because of excellent performance, copper and copper alloys are widely used in many industries including electrical, machinery, transportation and marine [1–3]. However, the exposure of copper has increased opportunities for corrosion and destruction. Especially in marine environments, the damage is particularly severe because of chloride ions [4–11]. It is worth noting that copper corrosion causes huge economic losses, energy losses, and safety issues. Therefore, it is significant and necessary to study corrosion inhibition in a neutral chloride solution. Furthermore, understanding the inhibition mechanism will help us to improve inhibition efficiency.

Currently, various methods have been used to inhibit the corrosion of copper and its alloys [12–16]. One of the most traditional and efficient methods uses organic matter as a corrosion inhibitor [17–19]. In recent years, many organics, including benzotriazole (BTA), thiazole, iminazole, pyrrodiazole and their derivatives, are used as inhibitors [20–24]. However, most organic compounds containing nitrogen, oxygen, phosphorus, and sulfur are difficult to dissolve in aqueous solution, and can also cause huge damage to environment. Considering toxicity and water solubility, the development of novel, environment-friendly corrosion inhibitors is urgent. Ionic liquids as green compounds have attracted

much attention because of their excellent properties. They are characterized by low toxicity, large electrochemical window, negligible vapor pressure, non-volatility, non-flammability, easy degradability, easily recyclability, and easily solubility in water. It has been reported that ionic liquids inhibit the corrosion of steel, but there is little research on copper [25–29]. In addition, the inhibition mechanism of ionic liquids is unclear. Based on the above considerations, this study was conducted.

Thiazolyl blue (MTT) composed with an organic cation and a bromide anion is expected to have a good corrosion resistance performance. The aim of this study is to research the corrosion inhibition performance and discuss the inhibition mechanism of thiazolyl blue (MTT) for copper in simulated seawater solution (3% NaCl) at 298 K. The inhibition efficiency was studied by electrochemical measurements. The surface roughness and morphology of copper are observed by atomic force microscopy (AFM) and scanning electron-microscopy (SEM). The inhibition mechanism was further researched by Fourier transform infrared spectral (FT-IR), X-ray photoelectron spectroscopy (XPS), and molecular dynamics simulation (MD). It is found that the MTT molecules form covalent bonds with copper by N and S atoms. The adsorption model is parallel from MD, which is the largest area of coverage. The adsorption forms a protective film that insulates the metal surface from the corrosion medium. Thus, the MTT shows excellent corrosion resistance. The present work gives us an in-depth understanding of the inhibition principles of corrosion inhibitor, which is significant to inhibit copper corrosion.

2. Materials and Experimental

2.1. Materials

Thiazolyl blue (MTT) ($C_{18}H_{16}BrN_5S$, Aladdin, 98.0%, Shanghai, China, as shown in Figure 1, and sodium chloride (Aladdin, 99.5%, Shanghai, China) were used without any purification. The test solution was 3% NaCl in the presence and absence of various MTT (0.05 mM, 0.2 mM, 0.5 mM, 1.0 mM and 5.0 mM). In contrast, the blank solution was only 3% NaCl. Before each experiment, the sample was polished with different sandpapers (400, 800, 1200, 2000, Lifeng Inc., Huizhou, China), then cleaned ultrasonically with distilled water and alcohol respectively, before drying. The temperature was controlled by an aqueous thermostat (Lichen Inc., Shanghai, China). The studied metal was pure copper (more than 99.5% Cu).
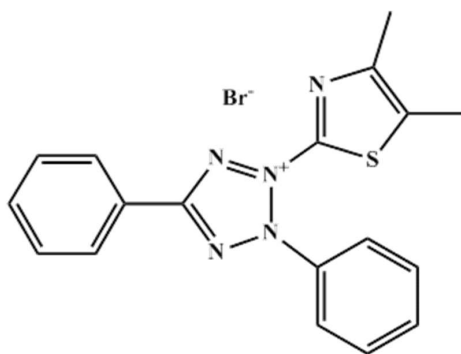

Figure 1. The Molecular structure of thiazolyl blue (MTT).

2.2. Electrochemical Measurements

The electrochemical workstation (CHI660C, Chenhua, Shanghai, China) was applied for the electrochemical experiments by a typical three-electrode system at 298 K. This electrode system consisted of a working electrode (WE, pure copper), the reference electrode (SCE, saturated calomel electrode), and counter electrodes (CE, platinum electrode). The area of the working electrode was 1 cm^2. At first, the copper electrode was at open circuit potential (OCP) for 1800 s to achieve a stable state. For electrochemical impedance spectroscopy (EIS) tests, the excitation signal amplitude was 5 mV,

the potential was OCP, and the range of frequency was $10^{-2} \sim 10^5$ Hz. Finally, the potentiodynamic polarization curves were performed with a scan rate of 0.5 mV/s, and the potential range of ± 250 mV versus the OCP. The inhibition efficiencies (η) from EIS and the polarization curves were calculated by (1) and (2) [30].

$$\eta = \frac{R_{\mathrm{p}} - R_{\mathrm{p},0}}{R_{\mathrm{p}}} \times 100\% \tag{1}$$

$$\eta = \left(\frac{I_{\mathrm{corr},0} - I_{\mathrm{corr}}}{I_{\mathrm{corr},0}} \right) \times 100\% \tag{2}$$

Here, I_{corr} and $I_{\mathrm{corr},0}$ represent corrosion current density, and R_{p} and $R_{\mathrm{p},0}$ represent polarization resistance with and without inhibitors. Besides, a durability test was performed, and the concrete results can be found in Figure S (see the Supplementary Materials).

2.3. Surface Analysis

The AFM (MFP-3D-BIO, Asylum Research, Goleta, CA, USA), the contact angle (JC2000C1, Zhongchen, Shanghai, China), and SEM (JSM-7800F, JEOL Ltd., Tokyo, Japan) were applied to further investigate copper appearance. The X-ray photoelectron spectroscopy (XPS, PHI 5700, Ulvac-Phi, Chigasaki, Japan) and the FT-IR (BRUKER, Bremen, Germany) measurements were employed to research the inhibition mechanism. The dimensions of the sample were 0.5 cm $\times$ 0.5 cm $\times$ 0.5 cm for SEM, and 1.00 cm $\times$ 1.00 cm $\times$ 0.1 cm for AFM, XPS, and FT-IR. Prior to each test, the specimens were immersed in a blank solution (3% NaCl) and 5 mM MTT test solution respectively for 24 h at 298 K before measurements. The contact angles were tested using the sessile water drop method. The XPS measurement was conducted with Al Kα X-ray source, and analyses were at an emitted photoelectron take-off angle of 90°. The binding energy scale was adjusted by the C1s of 284.8 eV and the XPS Peak 4.1 software was used to de-convolve all peaks using the Shirley-type background. For FT-IR, the pure substance (MTT) was compared with Cu-MTT film.

2.4. Calculation Methods

The theoretical calculations were carried out by Materials Studio software 8.0 (BIOVIA Inc., San Diego, CA, USA) to further research the inhibition mechanism. The quantum chemical calculations were achieved with DMol^3 module. The molecular structure was geometrically optimized with the density functional theory (DFT) and the B3LYP functional. The related parameters were obtained including dipole moment (μ), the lowest unoccupied molecular orbital (E_{LUMO}), the energy of highest occupied molecular orbital (E_{HOMO}), and the energy of and energy gap ($\Delta E_{\mathrm{Cu\text{-}inhibitor}} = E_{\mathrm{LUMO}} - E_{\mathrm{HOMO}}$). In addition, Forcite module was used to conduct the MD. The adsorption process between MTT cation and the Cu (111) surface was simulated in the aqueous phase with NVT ensemble, 1000 ps simulation time, and 1.0 fs time step at 298 K. The adsorption energy ($E_{\mathrm{Cu\text{-}inhibitor}}$) was calculated and analyzed by the equation [31].

$$E_{\mathrm{Cu-inhibitor}} = E_{\mathrm{Total}} - (E_{\mathrm{inhibitor}} + E_{\mathrm{Cu}}) \tag{3}$$

3. Results and Discussion

3.1. EIS Analysis

The EIS test was carried out to get information on corrosion inhibition performance. Figure 2 displays the Nyquist and bode curves with and without various concentrations of MTT for copper electrodes. The equivalent circuit models fitting the EIS experimental data are shown in Figure 3, and relevant parameters are shown in Table 1.

In Figure 3, the original lines are consistent with the fitting lines. Obviously, the Nyquist plots of the black and the lower concentration include a straight line at low frequencies and an oblate capacitive loop at high frequencies. According to corrosion resistance process, the capacitive loop attributes to

the charge transfer process (R_{ct}) and the double layer behavior (C_{dl}), where the dispersing effect results in the oblate semi-circle. In addition, the straight line at low frequency is the warburg impedance (*W*), which is related to the mass transportation between the copper surface and the bulk solution or the diffusion of oxygen [32]. However, the inductive loop disappears as the increase of MTT, indicating that the corrosion of copper is controlled by the charge transfer process [33]. It can be observed that the diameter of the semicircle increases with addition of MTT concentration, which suggests the inhibition performance is improved by the increase of MTT in an aggressive medium at 298 K. For the analysis of bode plots, the impedance value also increases for the whole frequency range. This phenomenon demonstrates that the inhibition performance increases with the augment of MTT. In addition, the shape of phase plots has changed: the two time constants are presented with the addition of MTT, leading us to speculate that the process of corrosion had changed [34]. It can be accepted that the MTT molecules form a protective film on copper by adsorption. Comparing the blank and MTT-modified electrodes, the phase angle at the high frequency is greater than 0 and closer to 90, which also indicates a protective film has formed on the copper surface [35].
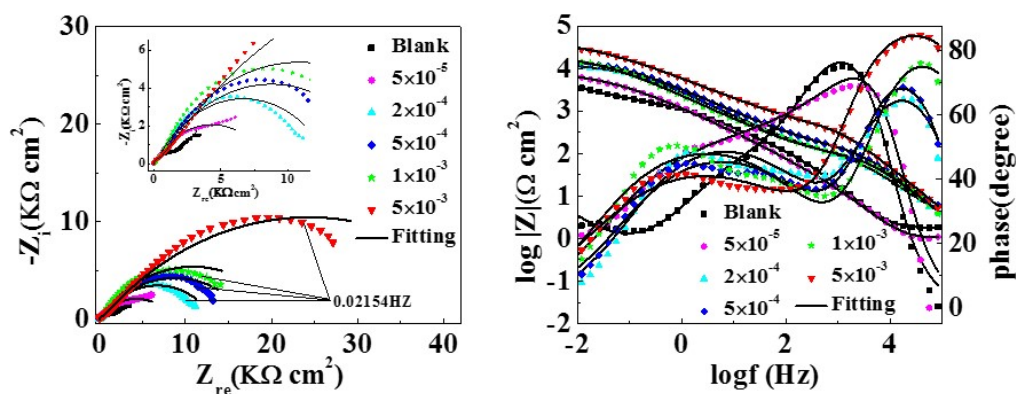

Figure 2. Nyquist and bode plots for the copper electrode with and without different concentrations of MTT in 3% NaCl at 298 K.
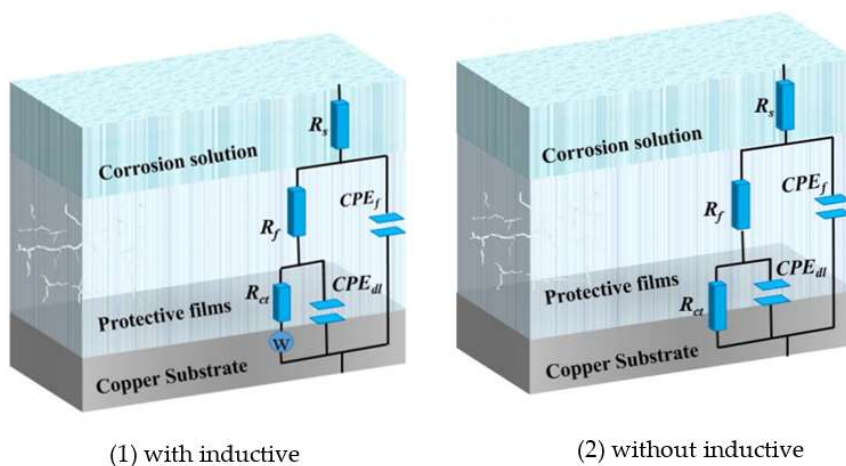

Figure 3. The equivalent circuits with and without inductive.

For equivalent circuits, R_p is the polarization resistance ($R_p = R_{ct} + R_f$), R_f represents the film resistance formed on the copper electrode surface, R_{ct} is the charge transfer resistance, Q_1 and Q_2 present the constant phase elements (CPE), C_f and C_{dl} are film capacitance and double-layer capacitance respectively. The CPE often represents pure capacitor, which is calculated from the following Equation (4) [36,37]:

$$Z_{CPE} = \frac{1}{Y(j\omega)^n} \tag{4}$$

Here, w is the angular frequency, n is the deviation parameter, Y is the CPE constant, and j is the imaginary root.

In Table 1, the values of C_{dl} and C_f decrease with the increase of MTT, which can be explained by Equations (5) and (6) [38]:

$$C_{dl} = \frac{\varepsilon^0 \varepsilon}{d} S \tag{5}$$

$$C_f = \frac{F^2 S}{4RT} \tag{6}$$

where S is the surface area of the electrode exposed to the corrosive solution, F is the Faraday's constant, ε^0 is the permittivity constant of the air, ε is the local dielectric constant of the film, and d is the thickness of the electric double layer. As more corrosion inhibitor molecules replace water molecules occupying the active sites with the increase of MTT concentration, which cause distinct electric double layer thickness increases, the area of copper electrode exposed to corrosion solution and local dielectric constant (ε) decreases [39]. The values of R_{ct} and R_p both have a reverse change, suggesting that the corrosion reaction is inhibited effectively. At the same time, the corrosion inhibition efficiency (η) increased with inhibitor concentration, the maximum efficiency is 95.73%. Furthermore, the durability of the Cu-MTT film is stable over a short period of time (<5 h) from durability tests. However, when the immersion time is more than 10 h, the protective effect of the film decreases slightly. This is due to corrosive substances in the solution, such as Cl^-, or unsound film.

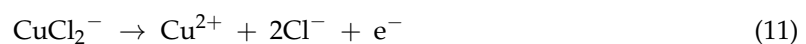**Table 1.** The related parameters of EIS for copper electrode in 3% NaCl at 298 K.

| | C (mM) | R_f (kΩ cm^2) | R_{ct} (kΩ cm^2) | R_p (Ω cm^2) | Q_1 | | Q_2 | | $W \times 10^{-3}$ (Ω cm^2) | η (%) |
					n_1	C_f (μF cm^{-2})	n_2	C_{dl} (μF cm^{-2})		
Blank	0	0.095	1.970	2.065	1	8.82	0.57	681.5	1.57	–
MTT	0.05	0.021	8.675	8.696	1	8.22	0.56	601.7	–	76.25
	0.2	0.104	13.260	13.364	0.88	2.57	0.60	106.3	–	84.55
	0.5	0.133	17.310	17.443	0.94	0.89	0.57	116.8	–	88.16
	1	0.089	21.580	21.669	0.94	0.96	0.59	213.8	–	90.47
	5	0.382	47.990	48.372	0.99	0.38	0.52	123.8	–	95.73

3.2. Potentiodynamic Polarization Curves Analysis

Figure 4 is the potentiodynamic polarization curves (Tafel) with and without different concentrations of MTT for copper in 3% NaCl at 298 K. The relevant parameters are obtained in Table 2. The cathodic reaction on copper surface in NaCl solution is Equation (7) [40]:

$$O_2 + 4e^- + 2H_2O \rightarrow 4OH^- \tag{7}$$

The anodic corrosion reaction follows (8)–(12) [41]:

$$Cu \rightarrow Cu^+ + e^- \tag{8}$$

$$Cu^+ + Cl^- \rightarrow CuCl \tag{9}$$

$$CuCl + Cl^- \rightarrow CuCl_2^- \tag{10}$$

$$CuCl_2^- \rightarrow Cu^{2+} + 2Cl^- + e^- \tag{11}$$

$$Cu^{2+} + Cu + 2Cl^- \rightarrow 2CuCl \tag{12}$$

In Figure 4, the maximum current density value (i_{peak}) is presented because of the corrosion of copper into Cu^+, as shown in Equation (8). As Equation (9) mentioned, the CuCl film is formed on

copper surface, the current density value shows the $I_{\min}$, and the corrosion is controlled provisionally. If the film is loose, the corrosion reaction will proceed further in chloride ion solution following Equations (10)–(12). With the addition of an inhibitor, a protective, dense film is formed on the surface of copper and corrosion is inhibited. Comparing with the blank, the values of I_{corr} decrease in the presence of MTT, which indicates that the copper corrosion is effectively inhibited. This phenomenon demonstrates that the addition of MTT not only inhibits the dissolution of oxygen, but also controls the corrosion of copper in an aggressive medium. In Table 2, β_c and β_a represent cathodic and anodic and Tafel slopes, respectively. The E_{corr} values move to a positive direction with a minimum moving value of 5 mM MTT, and all variation values lower than 85 mV; thus, the MTT can be defined as a mixed type inhibitor [42]. The corrosion inhibition ability is improved with the addition of the MTT concentration, which can be explained by the fact that more MTT molecules are absorbed on copper surface occupying the active sites to protect copper.
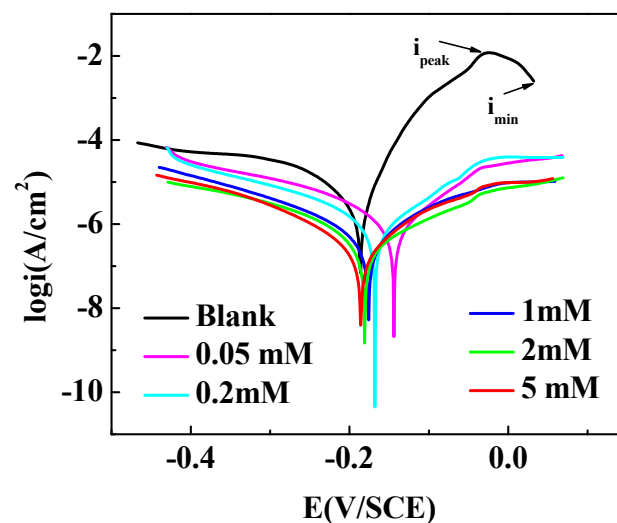
Figure 4. Polarization curves for copper with and without different concentrations of MTT in 3% NaCl at 298 K.

**Table 2.** The relevant parameters from polarization curve measurement.

|	C (mM)	E_{corr} (mV)	I_{corr} (A cm^{-2})	β_c (mV dec^{-1})	β_a (mV dec^{-1})	η (%)
Blank	0	−186	4.124×10^{-6}	−167.2	59.4	–
MTT	0.05	−144	1.073×10^{-6}	−149.7	78.4	73.98
	0.2	−168	1.010×10^{-6}	−159.2	78.2	75.51
	0.5	−176	5.877×10^{-7}	−138.1	128.7	85.75
	1	−181	4.559×10^{-7}	−149.1	124.5	88.95
	5	−186	3.184×10^{-7}	−117.7	118.4	92.28

3.3. Morphology Analysis

The SEM is considered as an important method for studying surface topography. The SEM and contact angle images of the copper samples with and without MTT are presented in Figure 5. The copper was seriously corroded in blank solution; as shown in Figure 5a, the surface becomes very rough and has many big pits. In contract, the copper surface is less damaged in 5 mM MTT solution (Figure 5b), which indicates that the MTT can prevent the copper from corroding in a neutral chloride solution. The surface of the sample treated with MTT becomes smoother than the blank, also suggesting that the copper is protected efficiently in an aggressive solution. In addition, the contact angle increases from 42.7° for Cu-Blank to 92.8° for Cu-MTT, which also demonstrates that the Cu-MTT film has hydrophobic property. The hydrophobicity gives rise to good corrosion inhibition performance.

The AFM 3D images and height plots of copper with and without MTT in 3% NaCl solution at 298 K are showed in Figure 6, which presents more information of copper appearance. Obviously, the blank (Figure 6a) shows a rough structure of the unprotected copper surface with large and deep pits, suggesting that the copper specimens are seriously corroded in a neutral chloride solution. As mentioned in previous reports, chloride ions seriously corrode copper. With the addition of MTT, the copper surface becomes smoother, as shown in Figure 6b, suggesting that MTT can inhibit the attack of corrosive ion to copper. The same conclusion can be drawn from the height plots. The average roughness (R_a) is 23.203 nm for the blank, as shown (Figure 6c), and the values of R_a reduce to 17.781 nm in the presence of MTT (Figure 6d), which indicates that the MTT can inhibit the copper corrosion in an aggressive medium. These results are in agreement with the above experiments.
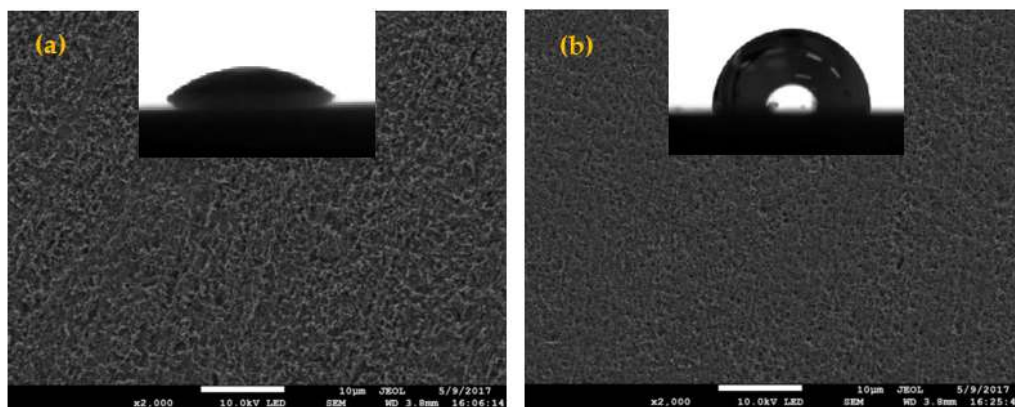
Figure 5. SEM and contact angle morphologies of the copper specimen immersed in 3% NaCl with and without MTT at 298 K ((**a**) the blank, (**b**) 5 mM MTT).
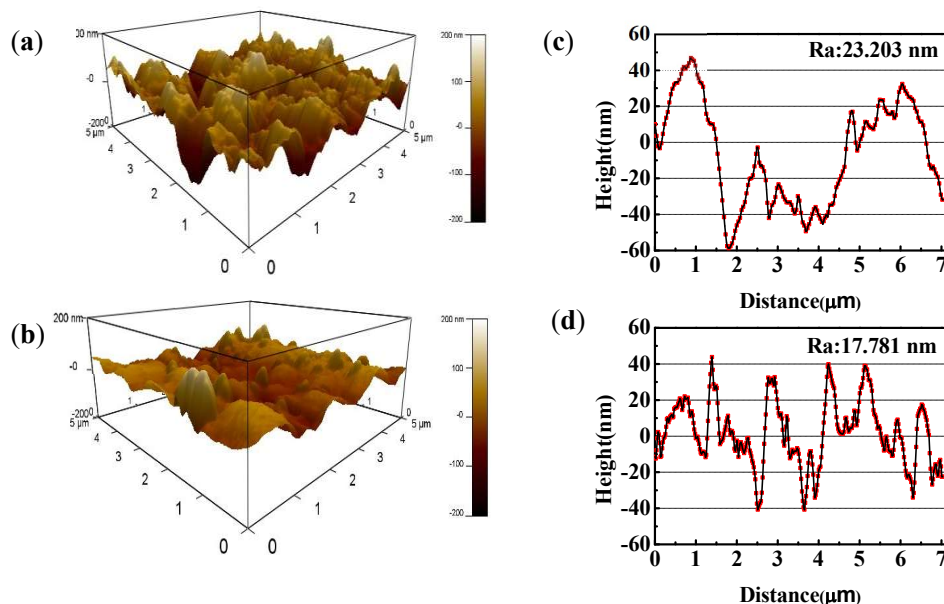

Figure 6. AFM morphologies of the copper specimen immersed in the blank solution with and without 5 mM MTT ((**a**,**c**) the blank, (**b**,**d**) 5 mM MTT).

3.4. FT-IR Spectra

To get more adsorption information, the FT-IR spectra of Cu-MTT film and pure MTT are compared in Figure 7. From the insets displayed in upper panels of Figure 7, it is obvious that the copper surface shows a darker colored film after immersion. For pure MTT, the bands

around 1605.3 cm^{-1}, 1460.5 cm^{-1} and 761.6 cm^{-1}are attributed to the C=N, C–N and phenyl ring, respectively [43]. There are analogous bands for Cu-MTT film in the same area, suggesting MTT molecules are adsorbed on copper. Furthermore, the bands of C=N and C–N both shift, and the relative adsorption intensity of C–N weakens compared to that of the pure MTT. Maybe there is a chemical interaction between MTT and copper. Then, the clathrate complex is formed on the surface of copper; this passive film can inhibit copper corrosion in aggressive medium. In order to explore the correlation between MTT and copper, the XPS measurement was performed.
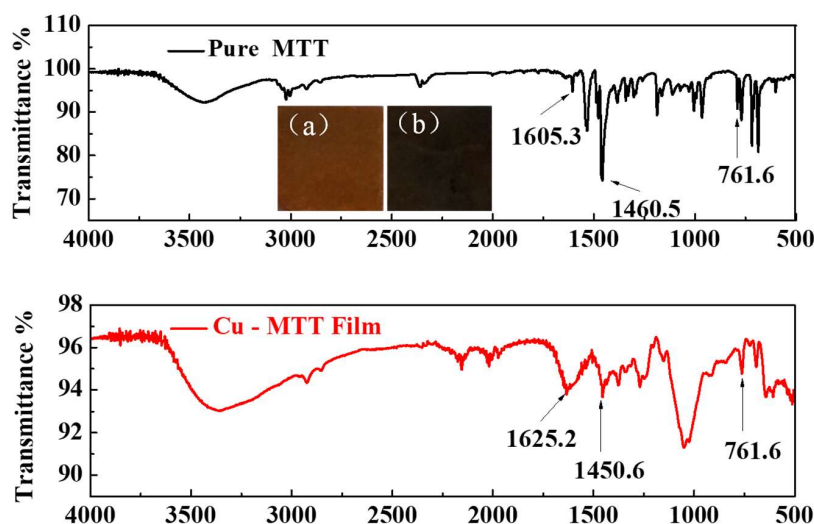
Figure 7. FT-IR spectra of MTT powder and Cu-MTT film. (Insets: morphologies for (**a**) pure copper and (**b**) after immersed in 5 mM MTT).

3.5. XPS Measurements

The XPS experiment was carried out to study the interaction between copper and MTT. Figure 8 compares the survey spectra for the Cu-blank and Cu-MTT film. C, O, and Cu exist in two samples, and N and S were detected on the Cu-MTT film, but not on the blank copper, which implies that MTT molecules can be absorbed by the copper surface, as mentioned above. Figure 9 shows the de-convolution XPS spectra of the blank (C1s, Cu2p, O1s) and Cu-MTT film (C1s, Cu2p, O1s, N1s and S2p). Correlative binding energy, full width at half maximum (FWHM), and chemical states are listed in Table 3.

In the survey spectra, a small amount of Cl was detected on the Cu-blank due to the CuCl from corrosion, but Cu-MTT was not detected. C, N, and S atomic content increases, suggesting the MTT molecules are absorbed on copper surface. However, O and Cu levels decrease for Cu-MTT, owing to the Cu-MTT film, which indicates the corrosion of copper is effectively inhibited.

For C1s de-convolution of the blank, the peaks at about 284.31 eV, 286.16 eV, and 287.70 eV are attributed to C–C/C–H, C–O–C and O–C=O respectively, which are caused by adventitious carbon pollution [44]. The corresponding peaks can be found in the Cu-MTT film. However, there is an obvious difference between the blank and Cu-MTT. The C=N/C–S (285.62 eV) and C–N (286.61 eV) can be found for Cu-MTT, but not for the blank. This phenomenon demonstrates that MTT molecules are absorbed on the copper surface in a corrosive solution.

It can be observed from the de-convolution spectra of Cu2p$_{3/2}$ that the peaks of Cu(0)/Cu(I) (913.9 eV, 913.95 eV) are contained for two samples. This results suggests that Cu(I) species (CuCl) are the main corrosion products in a neutral chloride solution [45]. Particularly, Cu(II) species are present on the Cu-MTT film, but not for the blank, which is attributed to the corrosion of Cu and the chemical interaction between MTT and copper. Furthermore, the relative intensity of Cu2p$_{3/2}$ for Cu-MTT is smaller compared with the blank, owing to the adsorption of MTT molecules.

For O1s, de-convolution of the blank and Cu-MTT, the O–C=O and C–C–C are due to adventitious oxygen contamination [46]. In Table 3, the lowest peaks, located at 530.14 eV, 530.65 eV, are copper oxide/cuprous oxide (CuO/Cu$_2$O) for the two copper samples [47]. The intensity of oxygen reduces because of the addition of MTT, suggesting the oxide of copper is restrained.
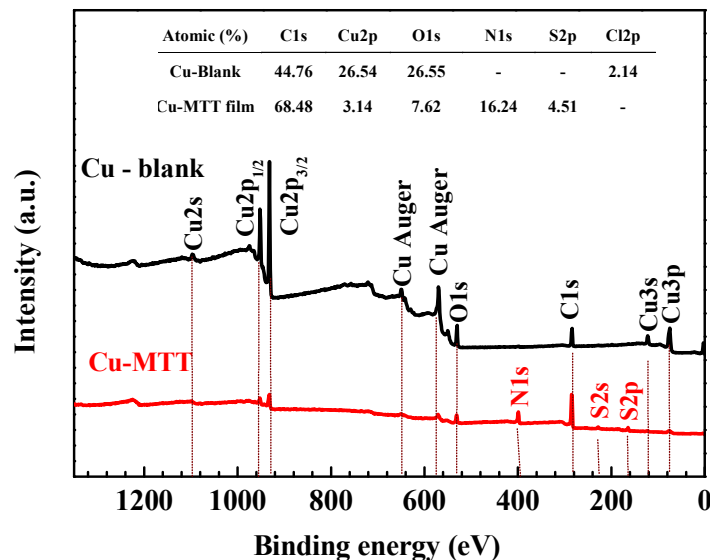
Atomic (%)	C1s	Cu2p	O1s	N1s	S2p	Cl2p
Cu-Blank	44.76	26.54	26.55	-	-	2.14
Cu-MTT film	68.48	3.14	7.62	16.24	4.51	-

Figure 8. Representative XPS survey spectra for the blank and Cu-MTT film.

Table 3. The homologous binding energy, chemical states and FWHM XPS spectra peaks from the surface of the blank and Cu-MTT film, respectively.

	The Blank			Cu-MTT		
	Chemical State	Binding Energy (ev)	FWHM	Chemical State	Binding Energy (ev)	FWHM
C1s	C–C/C–H	284.31	1.15	C–C/C–H	284.39	1.20
	C–O–C	286.16	1.15	C=N/C–S	285.62	1.20
	O–C=O	287.70	1.15	C–N	286.61	1.20
				O–C=O	287.71	1.20
Cu2p	Cu(0)/Cu(I)	931.90	1.13	Cu(0)/Cu(I)	931.95	1.7
				CuO	933.80	1.7
O1s	CuO/Cu$_2$O	530.14	1.00	CuO/Cu$_2$O	530.65	1.80
	O–C=O	531.30	1.00	O–C=O	531.98	1.80
	C–O–C	532.10	1.00	N=N	398.45	1.00
N1s				N=N	398.45	1.00
				N-N	399.20	1.00
				C=N	400.10	1.00
				C–N	400.70	1.00
				N:Cu	401.77	1.00
S2p				S–C	163.75	1.40
				S:Cu	165.07	1.40

The spectra of N1s for Cu-MTT are decomposed into the five peaks in Figure 9, suggesting five chemical forms of N atoms are presented on the copper surface. The type of peak at about 401.77 eV is the result of N:Cu from previous reports [48]. As shown in Table 3, four other peaks represent the type of MTT molecules [49]. As is well known, the nitrogen atom has a pair of lone pair electrons, which could be accepted by the unoccupied molecular orbital of Cu. Thus, it is commonly acceptable that the MTT are absorbed onto the copper surface by N atoms, which is in agreement with our FT-IR spectra analysis. For the spectra of S2p, the Cu-MTT sample contains two chemical states of S; the higher binding energy (165.07 eV) derived from S:Cu, which is a chemical bond between MTT and Cu [50]. The peak of S2p located at 163.75 eV corresponds to S–C from MTT, which also manifests that the MTT

is adsorbed on copper surface. It can be concluded that MTT molecules are absorbed chemically onto the copper surface by N and S atoms.
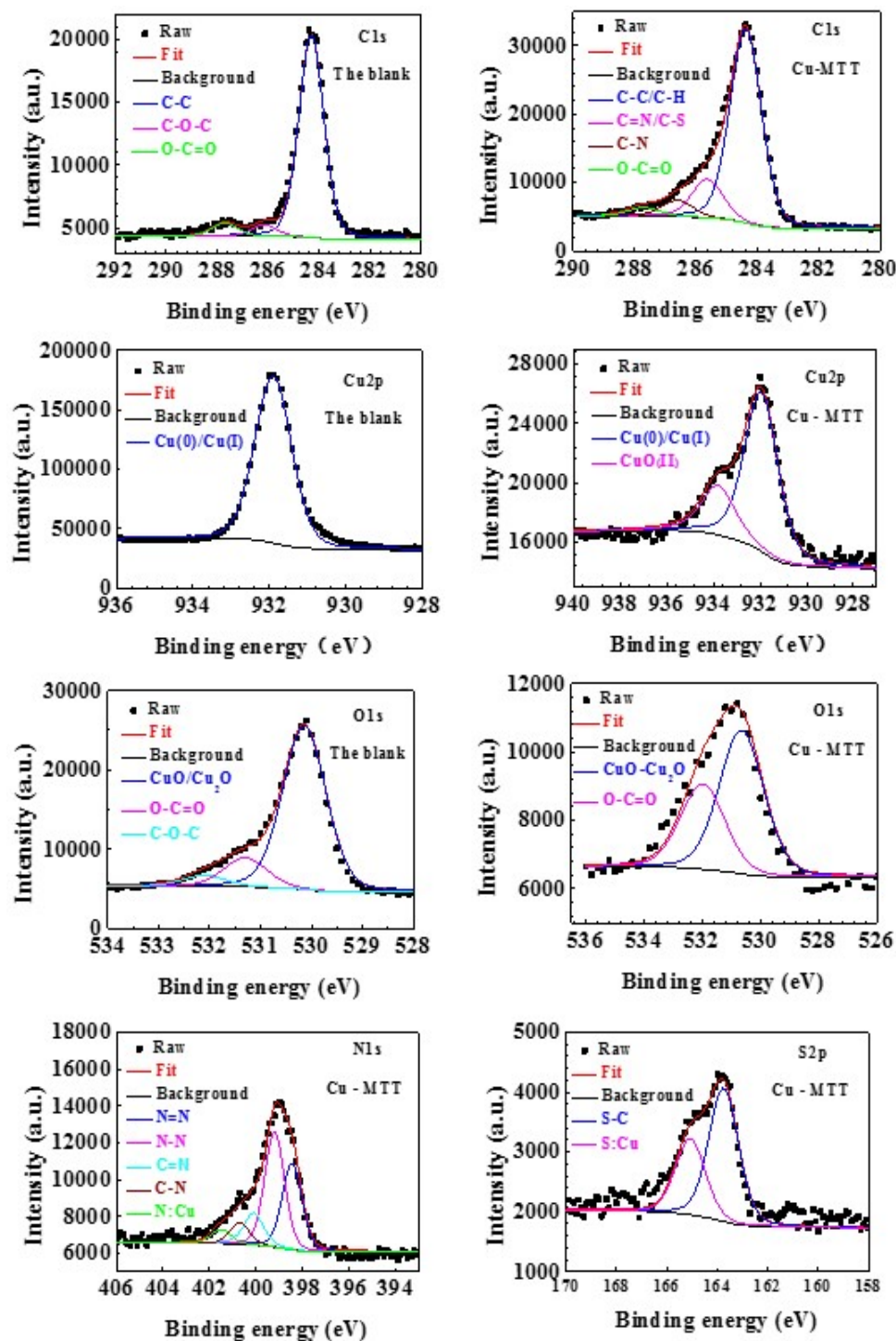

Figure 9. The de-convolution XPS spectra of for the blank and Cu-MTT film, respectively.

3.6. Adsorption Isotherm Analysis

In order to further study the adsorption process of inhibitor molecules on copper surface, various adsorption isotherms were applied to fit experimental data from Tafel and EIS data, as shown in Figure 10. The form of these isotherms is listed (13)−(17):

$$\text{Temkin adsorption isotherm: } KC \; = \; \exp(2a\theta) \tag{13}$$

$$\text{Frumkin adsorption isotherm: } \ln\left[\frac{\theta}{(1-\theta)C}\right] \; = \; \ln K \; + \; 2a\theta \tag{14}$$

$$\text{Flory-Huggins adsorption isotherm: } \ln\frac{\theta}{C} \; = \; x\ln(1-\theta) \; + \; \ln(xK_{ads}) \tag{15}$$

$$\text{EI-Awady adsorption isotherm: } \ln\frac{\theta}{1-\theta} \; = \; y\ln C \; + \; \ln K' \tag{16}$$

$$\text{Langmuir adsorption isotherm: } \frac{C}{\theta} \; = \; \frac{1}{K_{ads}} \; + \; c \tag{17}$$
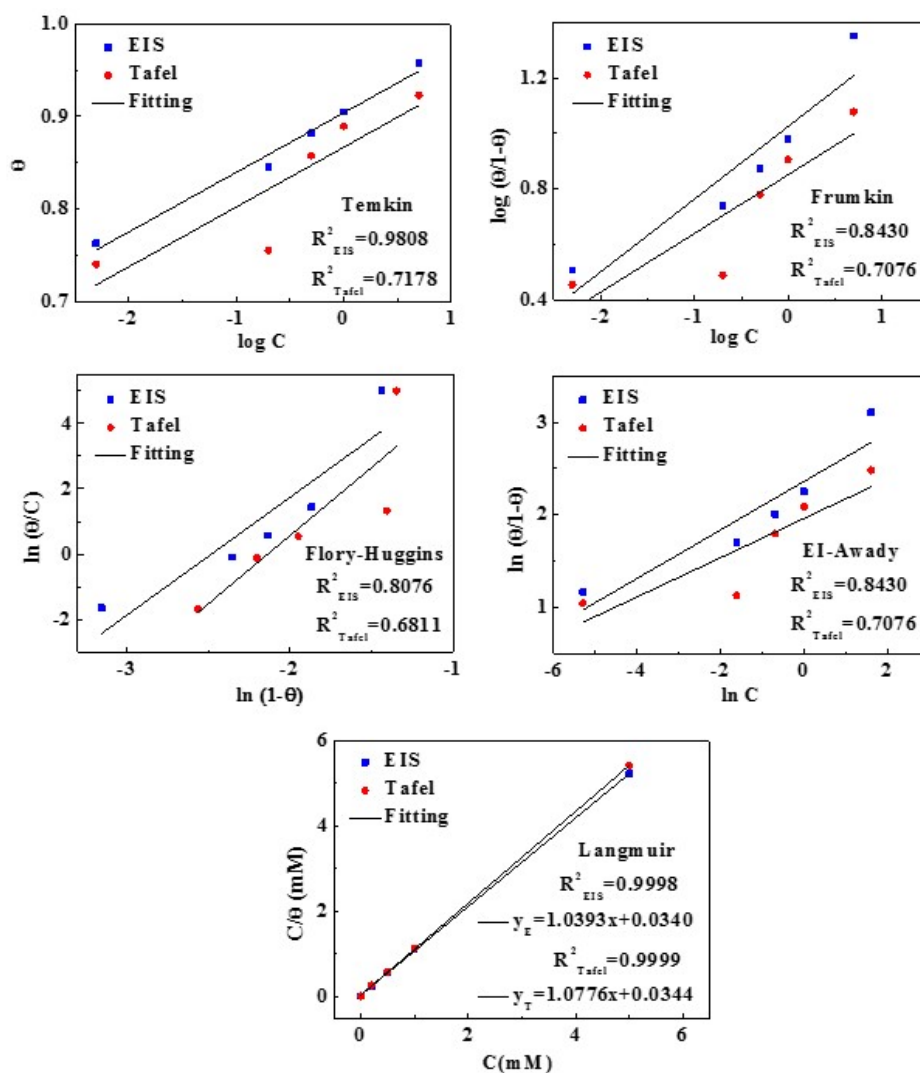
Figure 10. The various adsorption models fitting of MTT on copper surface.

For the adsorption behavior of MTT, the best description is Equation (17) named Langmuir adsorption. Here, θ is the surface coverage equaling the corrosion inhibition efficiency, and *C* is the inhibitor concentration. All linear regression coefficients (R^2) are clothing to 1, and all fitted results are in good agreement with the Langmuir adsorption. The relevant thermodynamic parameters are obtained in Table 4. The ΔG^0_{ads} is calculated by the Equation (18) [51]:

$$K_{\text{ads}} \;=\; \frac{1}{55.5} \exp\left(\frac{-\Delta G^0_{\text{ads}}}{RT}\right) \tag{18}$$

Generally speaking, a low value of ΔG^0_{ads} and a high value of K_{ads} manifest that inhibitors can be absorbed on metal strongly, showing better inhibitive behavior. The ΔG^0_{ads} values of MTT are negative, which suggests that the adsorption is spontaneous. In addition, the values of ΔG^0_{ads} range from $-20 \sim -40$ KJ/mol, which indicates the adsorption belongs to a mixed physical and chemical adsorption. If the value of ΔG^0_{ads} is closed to -40 KJ/mol, it is mainly chemical adsorption.

Table 4. The relevant thermodynamic parameters for copper from Langmuir adsorption isotherm.

| Measurements	K_{ads} ($\times 10^3$ L/mol)	ΔG^0_{ads} (KJ/mol)
Polarization	29.41	-35.44
EIS	29.07	-35.41

3.7. Theoretical Calculation

For the sake of investing the inhibition ability and behavior, the quantum chemical calculation is analyzed. The frontier molecular orbitals of MTT cation are displayed in Figure 11, including optimized geometric structure, the lowest unoccupied molecular orbital (LUMO), and the highest occupied molecular orbital (HOMO). Meanwhile, homologous parameters are obtained and analyzed. On the basis of the frontier orbital theory, the E_{HOMO} is often related to the ability of donating electrons, while the E_{LUMO} is associated with the electron-accepting ability [52–54]. In other words, the low E_{LUMO} (-0.259 eV) value and the high E_{HOMO} (-0.331 eV) value for present work mean a stronger electron-donating tendency. It suggests the MTT molecules more easily donates electron to copper to form a chemical bond. The higher dipole moment ($\mu = 20.50$ Debye) values and the lower energy gap values ($\Delta E = 0.072$ eV) of MTT reflect the higher inhibition efficiency [55,56]. In Figure 11, the HOMO and LUMO are mainly located at whole ring, suggesting whole molecular plane as active sites are absorbed on copper surface to form the protective film.
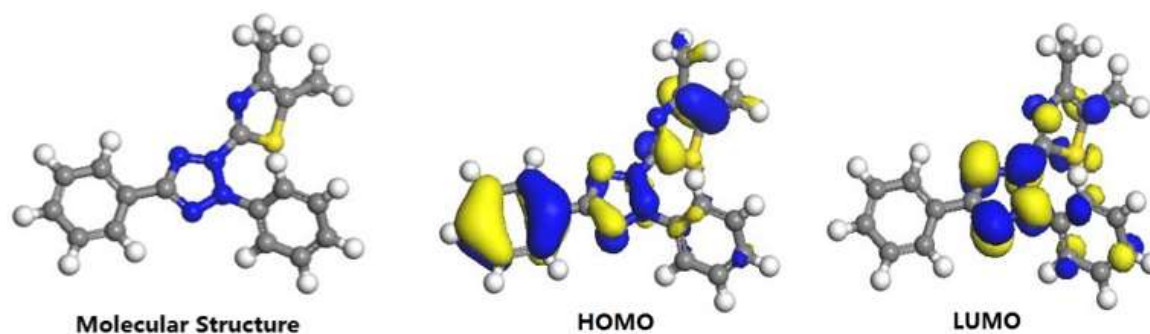
Figure 11. Optimized geometric structure and the frontier molecular orbital for the MTT cation.

The equilibrium configurations of MD (top view, side view) of MTT cation on copper surface are shown in Figure 12. Obviously, the MTT cation is adsorbed on copper surface by a parallel mode. This approach minimizes the copper area exposed to corrosive solution, showing good inhibition performance. The active sites from quantum chemical calculation also provide relevant evidence, thus showing perfect inhibition performance. For this adsorption, it is possible that the N and S atoms from MTT provide lone pair electrons to the empty d orbitals of copper forming the coordination bond. In addition, the lower interaction energy ($E_{\text{Cu-inhibitor}}$) value of -269.03 kcal mol^{-1} shows that MTT cations are strongly adsorbed on the surface of copper [57]. These results agree with experimental data.
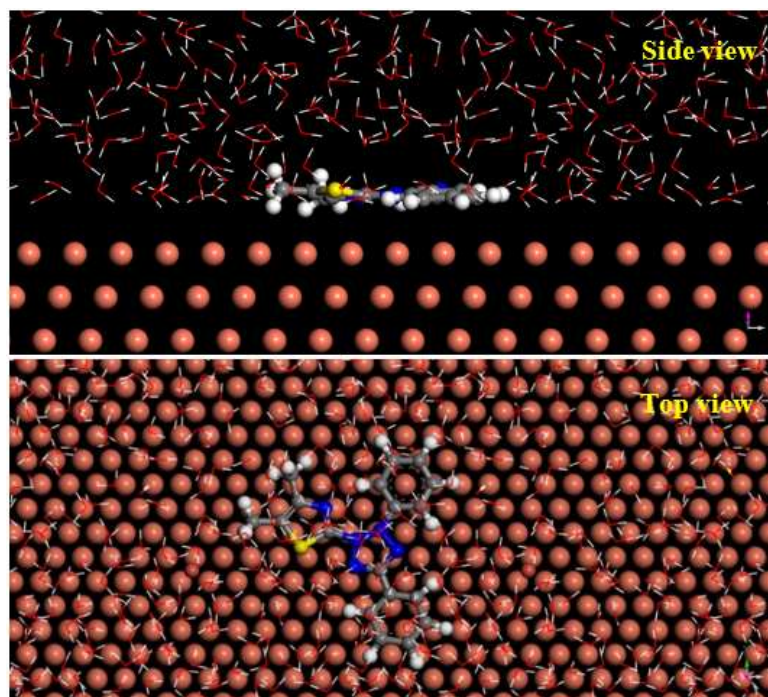
Figure 12. The equilibrium configuration of the molecular dynamics simulation for the MTT cation (**side view** and **top view**).

On the other hand, the halide ions (Cl$^-$, Br$^-$, I$^-$) have synergistic effects with some organic compounds for metal corrosion inhibition, according to previous reports [58,59]. Based on theoretical and experimental research, the inhibition mechanism of MTT in this study can be described, and is shown in Figure 13. Firstly, the negative bromine ions and chlorine ions are physically adsorbed onto the copper surface, and the MTT cations are adsorbed successively on copper surface by electrostatic interactions. This is thought to be physical adsorption. The adsorption of bromine and chlorine ions makes the copper surface positively charged. MTT cations with heteroatoms (N and S) form covalent bonds with copper easily, which is chemical adsorption. The FT-IR and XPS analysis concludes that the N and S atoms form covalent bonds with Cu, and the MD also provides relative evidence about adsorption, while the bromine element is not detected on the copper surface. This may be due to the fact that these ions are physically adsorbed onto the copper surface, or in small quantities.
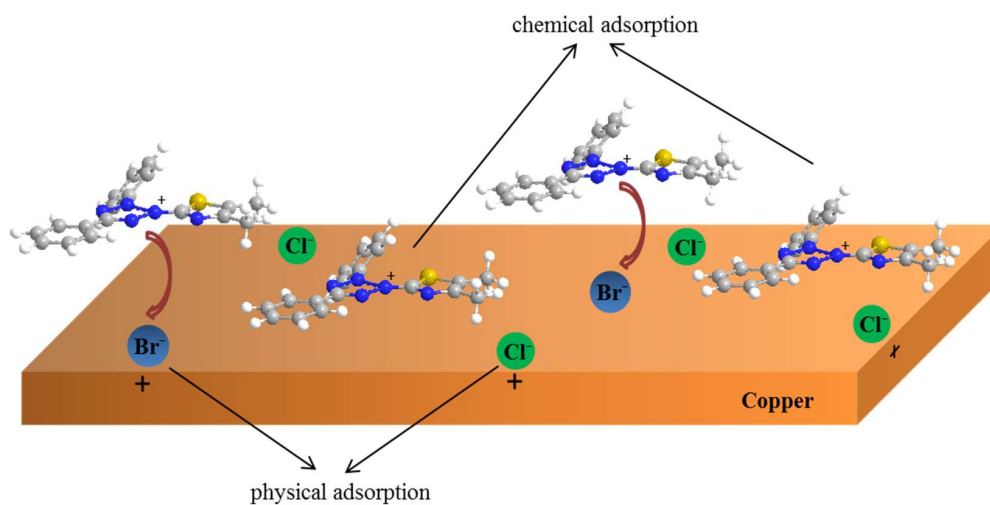
Figure 13. The corrosion inhibition mechanism diagram of MTT for copper in 3% NaCl solution.

4. Conclusions

Theoretical and experimental methods were applied to research the inhibition ability and inhibition mechanism. The following conclusions are obtained:

(1) The electrochemical tests, SEM, and AFM measurements demonstrate that the MTT as a mixed-type inhibitor can prevent copper corrosion effectively, and is efficiency increased with the addition of the MTT concentration.

(2) The MTT molecules form metal complex film by N and S atoms to inhibit corrosion from FT-IR spectra and XPS spectra.

(3) Adsorption isotherm studies demonstrated that adsorption for this work was a spontaneous mixed physical and chemical adsorption which obeyed Langmuir adsorption isotherm.

(4) The theoretical calculations reflected that MTT molecules processed a stronger adsorption on copper surface by a parallel mode, occupying the active site to the greatest extent by hydrophobic film, and thus, showing excellent inhibition effect.

References

1. Mousavi, M.; Baghgoli, T. Application of interaction energy in quantitative structure-inhibition relationship study of some benzenethiol derivatives on copper corrosion. *Corros. Sci.* **2016**, *105*, 170–176. [CrossRef]

2. Li, J.; Chen, D.; Zhang, D.; Wang, Y.; Yu, Y.; Gao, L.; Huang, M. Preparation of triazole compounds via click chemistry reaction and formation of the protective self-assembled membrane against copper corrosion. *Colloids Surf. A* **2018**, *550*, 145–154. [CrossRef]

3. Liu, W.; Xu, Q.; Han, J.; Chen, X.; Min, Y. A novel combination approach for the preparation of superhydrophobic surface on copper and the consequent corrosion resistance. *Corros. Sci.* **2016**, *110*, 105–113. [CrossRef]

4. Gerengi, H.; Mielniczek, M.; Gece, G.; Solomon, M.M. Experimental and quantum chemical evaluation of 8-Hydroxyquinoline as a corrosion inhibitor for copper in 0.1 M HCl. *Ind. Eng. Chem. Res.* **2016**, *55*, 9614–9624. [CrossRef]

5. Mo, S.; Luo, H.Q.; Li, N.B. Study on the influences of two thiazole flavor ingredients on Cu corrosion caused by chloride ion. *J. Colloid Interface Sci.* **2017**, *505*, 929–939. [CrossRef] [PubMed]

6. Tasić, Ž.Z.; Petrović Mihajlović, M.B.; Radovanović, M.B.; Simonović, A.T.; Antonijević, M.M. Cephradine as corrosion inhibitor for copper in 0.9% NaCl solution. *J. Mol. Struct.* **2018**, *1159*, 46–54. [CrossRef]

7. Ghelichkhah, Z.; Sharifi-Asl, S.; Farhadi, K.; Banisaied, S.; Ahmadi, S.; Macdonald, D.D. L-cysteine/polydopamine nanoparticle-coatings for copper corrosion protection. *Corros. Sci.* **2015**, *91*, 129–139. [CrossRef]

8. Hong, S.; Chen, W.; Zhang, Y.; Luo, H.Q.; Li, M.; Li, N.B. Investigation of the inhibition effect of trithiocyanuric acid on corrosion of copper in 3.0 wt.% NaCl. *Corros. Sci.* **2013**, *66*, 308–314. [CrossRef]

9. Wang, D.; Xiang, B.; Liang, Y.; Song, S.; Liu, C. Corrosion control of copper in 3.5 wt.% NaCl Solution by Domperidone: Experimental and Theoretical Study. *Corros. Sci.* **2014**, *85*, 77–86. [CrossRef]

10. Finšgar, M.; Kek Merl, D. An electrochemical, long-term immersion, and XPS study of 2-mercaptobenzothiazole as a copper corrosion inhibitor in chloride solution. *Corros. Sci.* **2014**, *83*, 164–175. [CrossRef]

11. Zheng, X.; Zhang, S.; Li, W.; Yin, L.; He, J.; Wu, J. Investigation of 1-butyl-3-methyl-1H-benzimidazolium iodide as inhibitor for mild steel in sulfuric acid solution. *Corros. Sci.* **2014**, *80*, 383–392. [CrossRef]

12. Cao, Y.; Dong, S.; Zheng, D.; Wang, J.; Zhang, X.; Du, R.; Song, G.; Lin, C. Multifunctional inhibition based on layered double hydroxides to comprehensively control corrosion of carbon steel in concrete. *Corros. Sci.* **2017**, *126*, 166–179. [CrossRef]

13. Chen, J.; Qin, Z.; Martino, T.; Shoesmith, D.W. Non-uniform film growth and micro/macro-galvanic corrosion of copper in aqueous sulphide solutions containing chloride. *Corros. Sci.* **2017**, *114*, 72–78. [CrossRef]

14. Yu, H.J.; Li, C.X.; Yuan, B.Y.; Li, L.; Wang, C. The inhibitive effects of AC-treated mixed self-assembled monolayers on copper corrosion. *Corros. Sci.* **2017**, *120*, 231–238. [CrossRef]

15. Zhou, Y.; Guo, L.; Zhao, Z.H.; Zheng, S.S.; Xu, Y.; Xiang, B.; Kaya, S. Anticorrosion potential of domperidone on copper in different concentration of hydrochloric acid solution. *J. Adhes. Sci. Technol.* **2018**, *32*, 1485–1502. [CrossRef]

16. Ma, X.; Xu, L.; Wang, W.; Lin, Z.; Li, X. Synthesis and characterisation of composite nanoparticles of mesoporous silica loaded with inhibitor for corrosion protection of Cu-Zn alloy. *Corros. Sci.* **2017**, *120*, 139–147. [CrossRef]

17. Nam, N.D.; Thang, V.Q.; Hoai, N.T.; Van Hien, P. Yttrium 3-(4-nitrophenyl)-2-propenoate used as inhibitor against copper alloy corrosion in 0.1 M NaCl solution. *Corros. Sci.* **2016**, *112*, 451–461. [CrossRef]

18. Kovacevic, N.; Milosev, I.; Kokalj, A. How relevant is the adsorption bonding of imidazoles and triazoles for their corrosion inhibition of copper? *Corros. Sci.* **2017**, *124*, 25–34. [CrossRef]

19. Wang, Z.; Gong, Y.; Jing, C.; Huang, H.; Li, H.; Zhang, S.; Gao, F. Synthesis of dibenzotriazole derivatives bearing alkylene linkers as corrosion inhibitors for copper in sodium chloride solution: A new thought for the design of organic inhibitors. *Corros. Sci.* **2016**, *113*, 64–77. [CrossRef]

20. Qafsaoui, W.; Kendig, M.W.; Joiret, S.; Perrot, H.; Takenouti, H. Ammonium pyrrolidine dithiocarbamate adsorption on copper surface in neutral chloride media. *Corros. Sci.* **2016**, *106*, 96–107. [CrossRef]

21. Li, M.; Xu, J.; Li, R.; Wang, D.; Li, T.; Yuan, M.; Wang, J. Simple preparation of aminothiourea-modified chitosan as corrosion inhibitor and heavy metal ion adsorbent. *J. Colloid Interface Sci.* **2014**, *417*, 131–136. [CrossRef] [PubMed]

22. Qiang, Y.; Zhang, S.; Yan, S.; Zou, X.; Chen, S. Three indazole derivatives as corrosion inhibitors of copper in a neutral chloride solution. *Corros. Sci.* **2017**, *126*, 295–304. [CrossRef]

23. Finšgar, M. 2-Mercaptobenzimidazole as a copper corrosion inhibitor: Part I. Long-term immersion, 3D-profilometry, and electrochemistry. *Corros. Sci.* **2013**, *72*, 82–89. [CrossRef]

24. Bokati, K.S.; Dehghanian, C.; Yari, S. Corrosion inhibition of copper, mild steel and galvanically coupled copper-mild steel in artificial sea water in presence of 1H-benzotriazole, sodium molybdate and sodium phosphate. *Corros. Sci.* **2017**, *126*, 272–285. [CrossRef]

25. Lozano, I.; Mazario, E.; Olivares-Xometl, C.O.; Likhanova, N.V.; Herrasti, P. Corrosion behaviour of API 5LX52 steel in HCl and H_2SO_4 media in the presence of 1,3-dibencilimidazolio acetate and 1,3-dibencilimidazolio dodecanoate ionic liquids as inhibitors. *Mater. Chem. Phys.* **2014**, *147*, 191–197. [CrossRef]

26. Ha, J.H.; Cho, J.-H.; Kim, J.H.; Cho, B.W.; Oh, S.H. 1-Butyl-1-methylpyrrolidinium chloride as an effective corrosion inhibitor for stainless steel current collectors in magnesium chloride complex electrolytes. *J. Power Sources* **2017**, *355*, 90–97. [CrossRef]

27. Feng, L.; Zhang, S.; Qiang, Y.; Xu, S.; Tan, B.; Chen, S. The synergistic corrosion inhibition study of different chain lengths ionic liquids as green inhibitors for X70 steel in acidic medium. *Mater. Chem. Phys.* **2018**, *215*, 229–241. [CrossRef]

28. Kannan, P.; Rao, T.S.; Rajendran, N. Anti-corrosion behavior of benzimidazoliumtetra fluroborate ionic liquid in acid medium using electrochemical noise technique. *J. Mol. Struct.* **2016**, *222*, 586–595.

29. Zheng, X.; Zhang, S.; Li, W.; Gong, M.; Yin, L. Experimental and theoretical studies of two imidazolium-based ionic liquids as inhibitors for mild steel in sulfuric acid solution. *Corros. Sci.* **2015**, *95*, 168–179. [CrossRef]

30. Mehmeti, V.V.; Berisha, A.R. Corrosion study of mild steel in aqueous sulfuric acid solution using 4-methyl-4H-1,2,4-triazole-3-thiol and 2-mercaptonicotinic acid-An experimental and theoretical study. *Front. Chem.* **2017**, *5*, 61. [CrossRef] [PubMed]

31. Guo, L.; Kaya, S.; Obot, I.B.; Zheng, X.; Qiang, Y. Toward understanding the anticorrosive mechanism of some thiourea derivatives for carbon steel corrosion: A combined DFT and molecular dynamics investigation. *J. Colloid Interface Sci.* **2017**, *506*, 478–485. [CrossRef] [PubMed]

32. Coelho, L.B.; Mouanga, M.; Druart, M.E.; Recloux, I.; Cossement, D.; Olivier, M.G. A SVET study of the inhibitive effects of benzotriazole and cerium chloride solely and combined on an aluminium/copper galvanic coupling model. *Corros. Sci.* **2016**, *110*, 143–156. [CrossRef]

33. Sigircik, G.; Yildirim, D.; Tuken, T. Synthesis and inhibitory effect of *N*,*N*′-bis(1-phenylethanol) ethylenediamine against steel corrosion in HCl Media. *Corros. Sci.* **2017**, *120*, 184–193. [CrossRef]

34. Hu, Z.; Meng, Y.; Ma, X.; Zhu, H.; Li, J.; Li, C.; Cao, D. Experimental and theoretical studies of benzothiazole derivatives as corrosion inhibitors for carbon steel in 1 M HCl. *Corros. Sci.* **2016**, *112*, 563–575. [CrossRef]

35. Metikos-Hukovic, M.; Babic, R.; Paic, I. Copper corrosion at various pH values with and without the inhibitor. *J. Appl. Electrochem.* **2000**, *30*, 617–624. [CrossRef]

36. Tian, H.W.; Li, W.H.; Hou, B.R.; Wang, D.P. Insights into corrosion inhibition behavior of multi-active compounds for X65 pipeline steel in acidic oilfield formation water. *Corros. Sci.* **2017**, *117*, 43–58. [CrossRef]

37. Kannan, P.; Rao, T.S.; Rajendran, N. Improvement in the corrosion resistance of carbon steel in acidic condition using naphthalen-2-ylnaphthalene-2-carboxammide inhibitor. *J. Colloid Interface Sci.* **2018**, *512*, 618–628. [CrossRef] [PubMed]

38. Mashuga, M.; Olasunkanmi, L.; Adekunle, A.; Yesudass, S.; Kabanda, M.; Ebenso, E. Adsorption, thermodynamic and quantum chemical studies of 1-hexyl-3-methylimidazolium based ionic liquids as corrosion inhibitors for mild steel in HCl. *Materials* **2015**, *8*, 3607–3632. [CrossRef]

39. Li, W.; Landon, J.; Irvin, B.; Zheng, L.F.; Ruh, K.; Kong, L.; Pelgen, J.; Link, D.; Figueroa, J.D.; Thompson, J.; et al. Use of Carbon Steel for Construction of Post-combustion CO_2 Capture Facilities: A Pilot-Scale Corrosion Study. *Ind. Eng. Chem. Res.* **2017**, *56*, 4792–4803. [CrossRef]

40. Qiang, Y.; Zhang, S.; Xu, S.; Yin, L. The effect of 5-nitroindazole as an inhibitor for the corrosion of copper in a 3.0% NaCl solution. *RSC Adv.* **2015**, *5*, 63866–63873. [CrossRef]

41. Song, P.; Guo, X.-Y.; Pan, Y.-C.; Shen, S.; Sun, Y.; Wen, Y.; Yang, H.-F. Insight in cysteamine adsorption behaviors on the copper surface by electrochemistry and Raman spectroscopy. *Electrochim. Acta* **2013**, *89*, 503–509. [CrossRef]

42. Coelho, L.B.; Cossement, D.; Olivier, M.G. Benzotriazole and cerium chloride as corrosion inhibitors for AA2024-T3: An EIS investigation supported by SVET and ToF-SIMS analysis. *Corros. Sci.* **2018**, *130*, 177–189. [CrossRef]

43. Stoian, D.; Bansode, A.; Medina, F.; Urakawa, A. Catalysis under microscope: Unraveling the mechanism of catalyst de- and re-activation in the continuous dimethyl carbonate synthesis from CO_2 and methanol in the presence of a dehydrating agent. *Catal. Today* **2017**, *283*, 2–10. [CrossRef]

44. Huang, H.; Wang, Z.; Gong, Y.; Gao, F.; Luo, Z.; Zhang, S.; Li, H. Water soluble corrosion inhibitors for copper in 3.5 wt.% sodium chloride solution. *Corros. Sci.* **2017**, *123*, 339–350. [CrossRef]

45. Wang, Y.; Lin, F.; Peng, J.; Dong, Y.; Li, W.; Huang, Y. A robust bilayer nanofilm fabricated on copper foam for oil–water separation with improved performances. *J. Mater. Chem. A* **2016**, *4*, 10294–10303. [CrossRef]

46. Zhang, J.; Liu, Z.; Han, G.-C.; Chen, S.-L.; Chen, Z. Inhibition of copper corrosion by the formation of Schiff base self-assembled monolayers. *Appl. Surf. Sci.* **2016**, *389*, 601–608. [CrossRef]

47. Welbourn, R.J.L.; Truscott, C.L.; Skoda, M.W.A.; Zarbakhsh, A.; Clarke, S.M. Corrosion and inhibition of copper in hydrocarbon solution on a molecular level investigated using neutron reflectometry and XPS. *Corros. Sci.* **2017**, *115*, 68–77. [CrossRef]

48. Wang, Y.; Liu, Z.; Huang, Y.; Qi, Y. The polymeric nanofilm of triazinedithiolsilane fabricated by self-assembled technique on copper surface. Part 2: Characterization of composition and morphology. *Appl. Surf. Sci.* **2015**, *356*, 191–202. [CrossRef]

49. Appa Rao, B.V.; Narsihma Reddy, M. Formation, characterization and corrosion protection efficiency of self-assembled 1-octadecyl-1H-imidazole films on copper for corrosion protection. *Arab. J. Chem.* **2017**, *10*, S3270–S3283. [CrossRef]

50. Yang, W.; Li, T.; Zhou, H.; Huang, Z.; Fu, C.; Chen, L.; Li, M.; Kuang, Y. Electrochemical and anti-corrosion properties of octadecanethiol and benzotriazole binary self-assembled monolayers on copper. *Electrochim. Acta* **2016**, *220*, 245–251. [CrossRef]

51. Wei, L.; Chen, Z.; Guo, X. Inhibition behavior of an imidazoline inhibitor for carbon steel in a supercritical CO_2/H_2O system. *J. Electrochem. Soc.* **2017**, *164*, C602–C609. [CrossRef]

52. Yu, Y.; Wang, Y.; Li, J.; Zhang, D.; Gao, L. In situ click-assembling monolayers on copper surface with enhanced corrosion resistance. *Corros. Sci.* **2016**, *113*, 133–144. [CrossRef]

53. Khalil, N. Quantum chemical approach of corrosion inhibition. *Electrochim. Acta* **2003**, *48*, 2635–2640. [CrossRef]

54. Frau, J.; Glossman-Mitnik, D. Conceptual DFT descriptors of amino acids with potential corrosion inhibition properties calculated with the latest minnesota density functionals. *Front. Chem.* **2017**, *5*, 16. [CrossRef] [PubMed]

55. Qiang, Y.; Zhang, S.; Guo, L.; Zheng, X.; Xiang, B.; Chen, S. Experimental and theoretical studies of four allyl imidazolium-based ionic liquids as green inhibitors for copper corrosion in sulfuric acid. *Corros. Sci.* **2017**, *119*, 68–78. [CrossRef]

56. Guo, L.; Safi, Z.S.; Kaya, S.; Shi, W.; Tüzün, B.; Altunay, N.; Kaya, C. Anticorrosive effects of some thiophene derivatives against the corrosion of iron: A computational study. *Front. Chem.* **2018**, *6*, 155. [CrossRef] [PubMed]

57. Zuriaga-Monroy, C.; Oviedo-Roa, R.; Montiel-Sanchez, L.E.; Vega-Paz, A.; Marin-Cruz, J.; Martinez-Magadan, J.M. Theoretical study of the aliphatic-chain length's electronic effect on the corrosion inhibition activity of methylimidazole-based ionic liquids. *Ind. Eng. Chem. Res.* **2016**, *55*, 3506–3516. [CrossRef]

58. Li, X.H.; Deng, S.D.; Fu, H.; Xie, X.G. Synergistic inhibition effects of bamboo leaf extract/major components and iodide ion on the corrosion of steel in H3PO4 solution. *Corros. Sci.* **2014**, *78*, 29–42. [CrossRef]

59. Guo, L.; Ou, Y.; Shen, X.; Kaya, S.; Shi, W.; Zhang, R.; Zheng, X.; Wang, J. Specific adsorption of halide ions on iron surface: A combined electrochemical and Monte Carlo simulation investigation. *Int. J. Electrochem. Sci.* **2017**, *12*, 7064–7074. [CrossRef]